

RESEARCH ARTICLE | OCTOBER 16 2023

Ratiometric luminescent thermometry for the third bioimaging window by Er³⁺ doped garnet with large Stark splitting

Shuaiqi Liu ; Jumpei Ueda ; Setsuhisa Tanabe  

 Check for updates

Appl. Phys. Lett. 123, 161101 (2023)

<https://doi.org/10.1063/5.0168845>



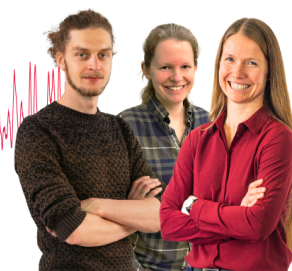
Webinar From Noise to Knowledge

May 13th – Register now



Zurich Instruments

Universität Konstanz



Ratiometric luminescent thermometry for the third bioimaging window by Er³⁺ doped garnet with large Stark splitting

Cite as: Appl. Phys. Lett. **123**, 161101 (2023); doi: 10.1063/5.0168845

Submitted: 21 July 2023 · Accepted: 1 October 2023 ·

Published Online: 16 October 2023



View Online



Export Citation



CrossMark

Shuaiqi Liu,¹  Jumpei Ueda,²  and Setsuhisa Tanabe^{1,a)} 

AFFILIATIONS

¹Graduate School of Human and Environmental Studies, Kyoto University, Kyoto 606-8501, Japan

²Graduate School of Advanced Science and Technology, Japan Advanced Institute of Science and Technology (JAIST), Ishikawa 923-1292, Japan

^{a)}Author to whom correspondence should be addressed: tanabe.setsuhisa.4v@kyoto-u.ac.jp

ABSTRACT

Based on the ${}^4I_{13/2} \rightarrow {}^4I_{15/2}$ emission (1450–1700 nm) of Er³⁺ in garnet, which is matching well with third bioimaging window (NIR-III), we propose a ratiometric near-infrared (NIR) thermometer (YAGG:Ce-Er) in NIR-III by utilizing thermal coupling between Stark levels of ${}^4I_{13/2}$, where energy levels were split into seven sublevels (I–VII). The energy gaps between Stark sublevel VII and I (ΔE_{VII-I}) and V and I (ΔE_{V-I}) of the ${}^4I_{13/2}$ level, calculated from the temperature dependence of intensity ratios of the two selected thermal couples, corresponded well with the theoretical values. This agreement supports the analysis that the system can be utilized as a Boltzmann thermometry. Moreover, the relative sensitivity (S_r) within the temperature range commonly encountered in organisms (25–60 °C) reached a value of $0.63 \pm 0.03\% \text{ K}^{-1}$ for the VII/I ratio and $0.57 \pm 0.07\% \text{ K}^{-1}$ for the V/I ratio. These high relative sensitivity values indicate the strong potential for practical application in various biological fields.

Published under an exclusive license by AIP Publishing. <https://doi.org/10.1063/5.0168845>

In recent years, there has been a great interest in the application of non-contact inorganic luminescent temperature probes utilizing the technique of luminescence intensity ratio (LIR).^{1–3} Unlike traditional thermometers that rely on direct contact and thermal expansion, these probes accurately measure and monitor temperature variations in different environments by utilizing the luminescent properties of inorganic materials that change with temperature. Inorganic luminescent probes, which possess high chemical stability, enable noninvasive, rapid, and accurate temperature measurements, thus avoiding the limitations of traditional contact sensors in terms of thermal resolution.^{4,5} Therefore, such thermometry probes provide many potential applications in various scientific and biological fields, such as microelectronics, catalysis, monitoring biological activities, and early cancer detection.^{6–9} Among them, the utilization of luminescent signals derived from two thermally coupled excited states of one luminescent center, known as the Boltzmann thermometers, continues to be regarded as one of the most reliable systems.¹⁰

Because of deeper biological tissue penetration depth, less tissue absorption and scattering, and better imaging effects, luminescent probes with operating at spectral ranges in the near-infrared (NIR) bioimaging window (BW) are more suitable for biological detection than that

working within visible light ranges (400–760 nm).^{11,12} The NIR BW is further divided into three segments: NIR-I (650–950 nm), NIR-II (1000–1350 nm), and NIR-III (1500–1800 nm).¹³ With longer wavelengths, particularly in the NIR-III range, the Rayleigh scattering (which varies with λ^{-4} , where λ is the wavelength) decreases, resulting in enhanced imaging contrast and signal-to-noise ratio.¹⁴ Furthermore, the recent development of affordable InGaAs detectors with sufficient sensitivity and high quantum efficiency in the range of 1000–1700 nm has made it possible to explore the potential of NIR-III luminescent probes in practical applications.¹⁵

The Er³⁺ ion is considered an excellent candidate of active center for achieving NIR-III Boltzmann thermometry due to its characteristic ${}^4I_{13/2} \rightarrow {}^4I_{15/2}$ transition in the range 1450–1650 nm, which aligns well with the NIR-III BW. Furthermore, the large Stark splitting of the ${}^4I_{13/2}$ level offers a potential solution by utilizing a Boltzmann thermometer based on the thermal coupling of its Stark sublevels. This approach enables the exploration and utilization of the Stark sublevels to accurately determine and quantify temperature variations within the NIR-III spectral range.

Here, we propose a ratiometric NIR thermometer (YAGG:Ce-Er) by utilizing thermal coupling between Stark-levels of ${}^4I_{13/2}$, where

energy levels were separated as seven sublevels.¹⁶ $Y_3Al_2Ga_3O_{12}$ garnet was chosen for its relatively strong crystal field strength and easy substitution of dodecahedral sites for Er^{3+} and Ce^{3+} .¹⁷ The incorporation of Ce^{3+} ions sensitize Er^{3+} by facilitating energy transfer from the $Ce^{3+}:^5d_1$ to the $Er^{3+}:^2H_{11/2}$ level.^{15,18,20} In addition, the extra addition of Cr^{3+} could achieve persistent luminescence in NIR-III by charging with UV to blue light, resulting in a potential thermometry without external excitation.¹⁵ Through the analysis of the deconvoluted twelve peaks originating from the $^4I_{13/2} \rightarrow ^4I_{15/2}$ transition, we have determined the energy difference (ΔE) between the two initial sublevels. The calculated ΔE , obtained from the intensity ratio of two selected thermal couples, aligns with the theoretical value, indicating the potential for future utilization of this NIR Boltzmann thermometer in bioimaging applications with temperature sensing.

The YAGG:Ce-Er ceramic phosphor with a composition of $Y_{2.925}Ce_{0.015}Er_{0.06}Al_2Ga_3O_{12}$ was synthesized by solid-state reactions. The chemicals used as raw materials were Y_2O_3 (99.99%), Al_2O_3 (99.99%), Ga_2O_3 (99.99%), Er_2O_3 (99.99%), and CeO_2 (99.99%). The powders were mixed with ethanol using a ball mill (Premium Line P-7, Fritsch, Idar-Oberstein, Germany) for 2 h. After drying the obtained slurry at 80 °C for 36 h, the mixed powder was pressed at 18 MPa to form a ceramic green body ($\Phi 10$ mm, 1 mm thickness) and finally sintered at 1600 °C for 10 h in a vacuum atmosphere. The temperature-dependent photoluminescence (PL) spectra were measured by pumping with a 405 nm laser diode (LD) (SDL-405-LM-100T, Shanghai Dream Lasers Technology Co. Ltd) using an InGaAs CCD spectrometer (NIR-Quest512, Ocean Optics) connected to an optical fiber. The spectra were measured from 900 to 1700 nm. To control the temperature, the ceramic sample was placed in a thermal stage (10035L, Japan High Tech) with a N_2 atmosphere from 100 to 500 K. All the spectra were calibrated into radiant flux using a standard halogen lamp (DH-2000-RECAL-EXT, Ocean Optics).

In order to assess the potential of the system as a ratiometric luminescent thermometer, the temperature dependence of the PL spectra was investigated between 5800 and 7200 cm^{-1} , corresponding to a wavelength range of 1389 to 1724 nm ($^4I_{13/2} \rightarrow ^4I_{15/2}$ transition of Er^{3+}), in the temperature range of 100–500 K (Fig. 1). The sample was excited by a 405 nm LD, and the PL spectra were recorded at intervals of 20 K. Figure 1 shows the observed PL bands for the $^4I_{13/2} \rightarrow ^4I_{15/2}$ transition, which is similar to that observed in the $Y_3Al_5O_{12}$ (YAG) host.^{19,20} The spectra exhibits distinct changes in trend with increasing temperature. Based on the different temperature dependence features, this figure can be divided into four periods: Range-1 (R1) ranging from approximately 6650 to 6900 cm^{-1} , Range-2 (R2) ranging from 6450 to 6650 cm^{-1} , Range-3 (R3) ranging from 6250 to 6450 cm^{-1} , and Range-4 (R4) ranging from 5975 to 6250 cm^{-1} . With increasing temperature, both the R1 and R3 intensities initially rise significantly and then reach a certain level, indicating their high initial Stark sublevels. However, the intensities of the lower energy portions, R1 (around 6750 cm^{-1}) and R3, decline when the temperature reaches approximately 280 K, suggesting a relatively low initial position due to the quenching effect. On the other hand, although the intensity of R2 and R4 at 500 K drops dramatically compared to low temperatures, indicating low initial levels R2 at around 6525 and 6590 cm^{-1} does not monotonically decrease with increasing temperature, indicating different initial levels.

Based on the analysis of temperature-dependent PL spectra and the specific energy position of Stark sublevels of Er^{3+} in YAG,²⁰ the

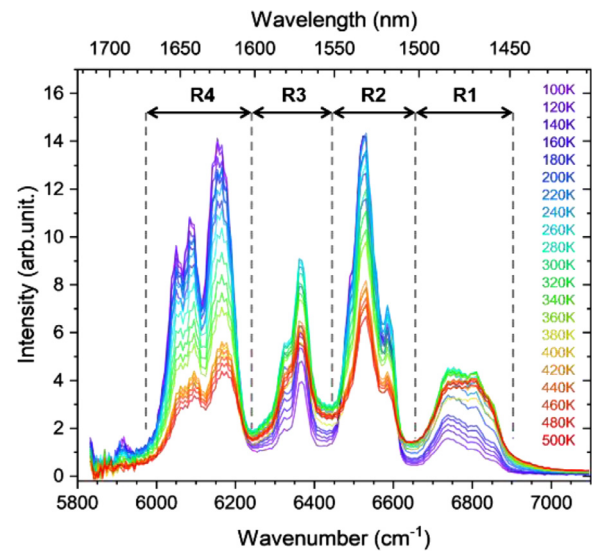


FIG. 1. Temperature dependence of the PL spectra of Er^{3+} doped garnet sample in the 100–500 K range under 405 nm LD excitation.

energy structure was evaluated, and an energy level diagram of Er^{3+} was derived as illustrated in Fig. 2(a). A cross-relaxation process occurs from $Er^{3+}:^4I_{11/2} \rightarrow ^4I_{13/2}$ to $Ce^{3+}:^2F_{7/2} \leftarrow ^2F_{5/2}$, resulting in the $^4I_{13/2} \rightarrow ^4I_{15/2}$ emission and quenching of the $^4I_{11/2} \rightarrow ^4I_{15/2}$ transition luminescence at 1.0 μm .^{15,22} The energy positions of the Stark sublevels of $^4I_{13/2}$ and $^4I_{15/2}$ are also shown in this figure, illustrating the initial and terminal states of each of the eleven peaks. The seven Stark sublevels of $^4I_{13/2}$ are denoted by roman numerals (I–VII), while the eight Stark sublevels of $^4I_{15/2}$ are denoted by arabic numerals (1–8). The emission peaks, from left to right, follow the order of decreasing energy [for example, VII(1) is the highest energy peak, while I(7) is the lowest energy peak].

To evaluate temperature dependence of each component, the peak deconvolution was done and the deconvoluted spectra at 100 and 300 K are presented in Fig. 2(b), combining the analysis of intensity changes for each peak and the temperature dependence observed in Fig. 1. The minor peak at about 5925 cm^{-1} , which may have resulted from external effects, was included to achieve a better fit. Peaks with an initial state of the IV level exhibited noticeable quenching effects at high temperatures compared to those originating from the V and VII levels. Conversely, the I level can be characterized by a monotonically declining intensity with increasing temperature. The different trend was observed for the II and III levels. With increasing temperature, the emission at approximately 6865 cm^{-1} due to VII(1) and 6755 cm^{-1} due to V(1) transition increased significantly in comparison with the emissions around 6162, 6091, and 6051 cm^{-1} corresponding to the transitions of I(5), I(6), and I(7), respectively. Indeed, the luminescence intensity ratio of the transitions related to the thermometric parameter should follow the Boltzmann law, as given by the following equations:

$$LIR_{VII/I} = \frac{I_{VII(1)}}{I_{I(5)} + I_{I(6)} + I_{I(7)}} = B_{VII-I} \exp\left(-\frac{\Delta E_{VII-I}}{k_B T}\right), \quad (1)$$

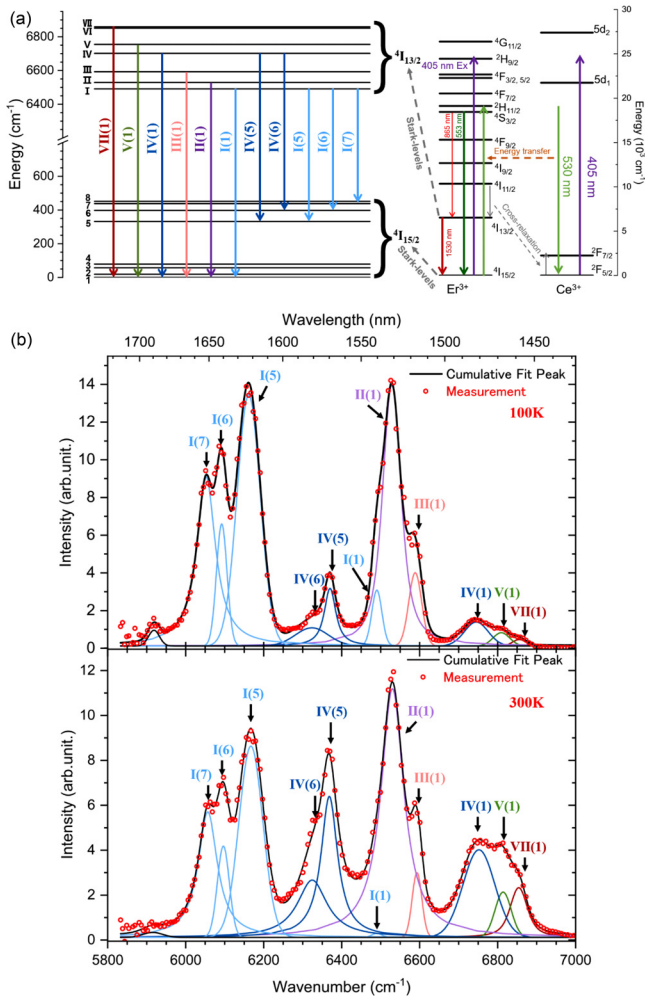


FIG. 2. (a) Energy level diagram of the Ce³⁺ and Er³⁺ in YAGG with Stark sublevels of ⁴I_{13/2} and ⁴I_{15/2} and (b) spectral deconvoluted eleven peaks of the PL spectra at 100 and 300 K.

$$LIR_{V/I} = \frac{I_{V(1)}}{I_{I(5)} + I_{I(6)} + I_{I(7)}} = B_{V-I} \exp\left(-\frac{\Delta E_{V-I}}{k_B T}\right), \quad (2)$$

where ΔE_{VII-I} and ΔE_{V-I} are the energy gap between the Stark sublevels of VII, V, and I, respectively, and k_B is the Boltzmann constant. Here,

$$B_{VII-I} = \frac{g_{VII} h \nu_{VII} A_{VII}}{g_I h \nu_I A_I}, \quad (3)$$

$$B_{V-I} = \frac{g_V h \nu_V A_V}{g_I h \nu_I A_I}, \quad (4)$$

where g_i , A_i , and ν_i are the degeneracy of the emitting level i , the spontaneous emission rate and the frequency of the transition from the excited state i to the ground state, respectively.¹⁰

To further evaluate the Boltzmann characteristics of two kinds of radiometric thermometry, the logarithm of the LIR between VII and

I ($LIR_{VII/I}$), V and I excited levels ($LIR_{V/I}$) were plotted vs T^{-1} in Fig. 3(a). According to the Boltzmann distribution in Eq. (1), the energy gaps, ΔE_{VII-I} and ΔE_{V-I} , between excited levels VII, V, and I can be determined by the slopes of linear fitting, $-\frac{\Delta E_{VII-I}}{k_B}$ and $-\frac{\Delta E_{V-I}}{k_B}$. Both logarithmic intensity ratio curves exhibit obvious deviations at lower temperatures due to weak thermal coupling, but good linearity is achieved above approximately 200 K. Thus, two types of combinations (VII/I and V/I) were linear fitted in the range of 200–500 K. In addition, the energy gaps ΔE_{VII-I} (373 cm⁻¹) and ΔE_{V-I} (276 cm⁻¹) calculated from the slopes of the Arrhenius plots are in agreement with the energy gaps estimated from the position of Stark sublevels, which are 374 and 264 cm⁻¹, respectively. This agreement indicates the reliability of the analysis as a Boltzmann thermometer.

To discuss the thermometric performances of the thermometers, two parameters of the absolute sensitivity S_a and the relative sensitivity S_r are given by the following equations:

$$S_a = \left| \frac{\partial LIR}{\partial T} \right|, \quad (5)$$

$$S_r = \frac{1}{LIR} \left| \frac{\partial LIR}{\partial T} \right|. \quad (6)$$

The plots of calculated S_a and S_r values for the two thermometric combinations are shown in Fig. 3(b). In quantifying and comparing the sensitivity of different thermometers, both S_a and S_r are important

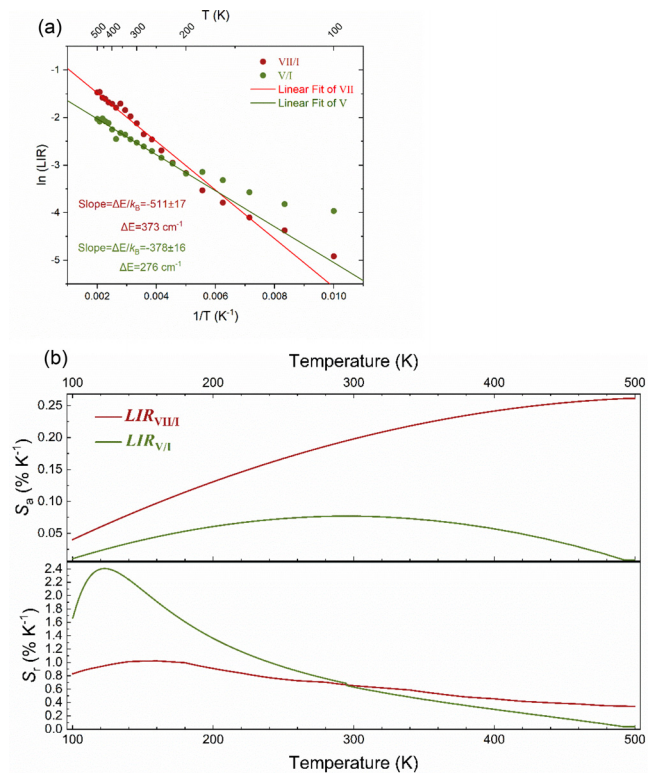


FIG. 3. (a) Arrhenius plot of LIR . The red and green lines represent the linear fitting of VII/I and V/I, respectively. (b) Temperature dependence of the absolute sensitivity and relative sensitivity of two couples.

parameters. Although S_a shows relatively small values across the entire temperature range, S_r demonstrates significantly high values for this sample. It was observed that the maximum S_r are $1.02\% \text{ K}^{-1}$ at 160 K and $2.41\% \text{ K}^{-1}$ at 120 K for VII/I and V/I, respectively. Furthermore, considering the requirements for *in vivo* imaging for studying biology, phosphors used as thermometry probes in organisms commonly operate within the range of 25–60 °C (298–333 K).^{21,22} Thus, taking this into consideration, when comparing the sample with the previous work reported by Wang *et al.* (a NIR-III thermometer constructed by doping Yb, Er, and Cr into a YAG host, which showed S_r as high as $0.276\% \pm 0.022\% \text{ K}^{-1}$ in this temperature range), our sample shows relatively high S_r values, averaging $0.63\% \pm 0.03\% \text{ K}^{-1}$ for VII/I and $0.57\% \pm 0.07\% \text{ K}^{-1}$ for V/I, respectively.²² The different S_r value was mostly due to different ΔE and our precise deconvolution analysis, which determined the precise population of each Stark level. With relatively high S_r value in the physiological temperature range, the sample is expected to be applied for biological temperature sensing.

In summary, a singly activated ratiometric Boltzmann luminescent thermometer based on the thermal coupling between Stark sublevels from the ${}^4I_{13/2} \rightarrow {}^4I_{15/2}$ transition of Er^{3+} in the YAGG host was designed to operate in the third bioimaging window. The entire emission was deconvoluted into twelve emission bands characterized by specific excited and terminal levels. The calculated energy gaps obtained from the ratio of two types of combinations (VII/I and V/I) are in good agreement with theoretical values. Moreover, the S_r values for both modes of logarithmic intensity ratio thermometry are remarkably high, reaching up to $0.63\% \pm 0.03\%$ and $0.57\% \pm 0.07\% \text{ K}^{-1}$ within the physiological temperature range of 25–60 °C. These results demonstrate the satisfactory performance of utilizing Stark sublevels in YAGG:Ce-Er as a ratiometric Boltzmann luminescent thermometer in the NIR-III.

The authors would like to thank the Research Grant from the Nippon Sheet Glass Foundation for Material Science and Engineering.

AUTHOR DECLARATIONS

Conflict of Interest

The authors have no conflicts to disclose.

Author Contributions

Shuaiqi Liu: Data curation (lead); Formal analysis (lead); Investigation (lead); Visualization (lead); Writing – original draft (lead).

Jumpei Ueda: Conceptualization (supporting); Supervision (supporting); Writing – review & editing (supporting). **Setsubisa Tanabe:** Conceptualization (lead); Funding acquisition (lead); Supervision (lead); Writing – review & editing (lead).

DATA AVAILABILITY

The data that support the findings of this study are available from the corresponding author upon reasonable request.

REFERENCES

- C. D. S. Brites, S. Balabhadra, and L. D. Carlos, *Adv. Opt. Mater.* **7**, 1801239 (2018).
- B. Dong, B. Cao, Y. He, Z. Liu, Z. Li, and Z. Feng, *Adv. Mater.* **24**, 1987–1993 (2012).
- Z. Wang, H. Jiao, and Z. Fu, *Inorg. Chem.* **57**, 8841–8849 (2018).
- X. Wang, O. S. Wolfbeis, and R. J. Meier, *Chem. Soc. Rev.* **42**, 7834–7869 (2013).
- A. Skripka, A. Benayas, R. Marin, P. Canton, E. Hemmer, and F. Vetrono, *Nanoscale* **9**, 3079–3085 (2017).
- O. Yarimaga, S. Lee, D. Y. Ham, J. M. Choi, S. G. Kwon, M. Im, S. Kim, J. M. Kim, and Y. K. Choi, *Macromol. Chem. Phys.* **212**, 1211–1220 (2011).
- J. Zhou, Q. Liu, W. Feng, Y. Sun, and F. Li, *Chem. Rev.* **115**(1), 395–465 (2015).
- R. G. Geitenbeek, A. E. Nieuwelink, T. S. Jacobs, B. B. V. Salzmans, J. Goetze, A. Meijerink, and B. M. Weckhuysen, *ACS Catal.* **8**, 2397–2401 (2018).
- D. Jaque and F. Vetrono, *Nanoscale* **4**, 4301–4326 (2012).
- M. Back, J. Ueda, M. G. Brik, T. Lesniewski, M. Grinberg, and S. Tanabe, *ACS Appl. Mater. Interfaces* **10**, 41512–41524 (2018).
- R. R. Anderson and J. A. Parrish, *J. Invest. Dermatol.* **77**, 13 (1981).
- K. Soga, K. Tokuzen, K. Fukuda, H. Hyodo, E. Hemmer, N. Venkatachalam, and H. Kishimoto, *J. Photopolym. Sci. Technol.* **25**, 57 (2012).
- E. Hemmer, N. Venkatachalam, H. Hyodo, A. Hattori, Y. Ebina, H. Kishimoto, and K. Soga, *Nanoscale* **5**, 11339–11361 (2013).
- A. M. Smith, M. Mancini, and S. Nie, *Nat. Nanotechnol.* **4**, 710–711 (2009).
- J. Xu, D. Murata, J. Ueda, and S. Tanabe, *J. Mater. Chem. C* **4**, 11096 (2016).
- J. A. Koningstein and J. E. Geusic, *Phys. Rev.* **136**, A726 (1964).
- P. Dorenbos, *J. Lumin.* **134**, 310–318 (2013).
- Y. Shiota, S. Tanabe, T. Hanada, and Y. Maeda, *J. Ceram. Soc. Jpn.* **107**(12), 1201–1205 (1999).
- J. Meng, K. Cheah, Z. Shi, and J. Li, *Appl. Phys. Lett.* **91**, 151107 (2007).
- M. Nishi, S. Tanabe, K. Fujita, and K. Hirao, *J. Alloys Compd.* **408–412**, 788–790 (2006).
- H. Peng, M. I. J. Stich, J. Yu, L. Sun, L. H. Fischer, and O. S. Wolfbeis, *Adv. Mater.* **22**, 716–719 (2010).
- Z. Wang, M. Jia, M. Zhang, X. Jin, H. Xu, and Z. Fu, *Inorg. Chem.* **60**(19), 14944–14951 (2021).